Journal of Geophysical Research: Biogeosciences

Supporting Information for

How turbidity currents dictate organic carbon fluxes across river-fed fjords

S. Hage[1,2,3*], V.V. Galy[4], M.J.B. Cartigny[5], C. Heerema[5], M.S. Heijnen[6], S. Acikalin[7], M.A. Clare[6], I. Giesbrecht[8], D.R. Gröcke[9], A. Hendry[7], R. G. Hilton[5,10], S.M. Hubbard[1], J.E. Hunt[6], D.G. Lintern[11], C. McGhee[7], D.R. Parsons[12], E. L. Pope[5], C D. Stacey[11], E.J. Sumner[3], S. Tank[8], P.J. Talling[5]

[1]Department of Geoscience, University of Calgary, Canada

[2]Géosciences Marines, Ifremer, France

[3]School of Ocean and Earth Sciences, University of Southampton, UK

[4]Department of Marine Chemistry and Geochemistry, Woods Hole Oceanographic Institution

[5]Department of Geography, Durham University, UK[6]National Oceanography Centre Southampton, UK

[7]School of Natural and Environmental Sciences, Newcastle University, UK

[8]Hakai Institute, Victoria, BC, Canada,

[9]Department of Earth Sciences, Durham University, UK

[10]Department of Earth Sciences, University of Oxford, UK

[11]Geological Survey of Canada, Natural Resources Canada, Sidney, British Columbia

[12]Energy and Environment Institute, University of Hull, UK

*Corresponding author: Sophie Hage (sophie.hage@ifremer.fr)

Contents of this file

Introduction

The following information contains supplementary description of the methods used to estimate the river flow and sediment discharge (Text S1 to S3), and the approaches used to determine sedimentation rates in the seabed of Bute Inlet (Text S4 and S5). Five supplementary figures, five equations and five tables are also included.

Text S1: Flow discharge of Homathko and Southgate Rivers

The Homathko River has been gauged by Water Survey of Canada for decades while the Southgate River was not gauged until late June 2021 (Fig. S1). Therefore, in order to estimate the Southgate discharge in our year of sampling (2017), we developed a linear regression model that predicted Southgate discharge from Homathko discharge using all available overlapping flow observations as of late October 2021 (Fig. S2a). The training dataset contained n = 123 daily flow observations spanning a broad range of flows from record high discharge in late June 2021 through moderately low flows in October 2021. The resulting model had a good overall fit (10 fold cross-validated RMSE = 22.2; R^2 = 0.98; Fig. S2b) and was used to backcast Southgate River discharge for 2017 (Fig. S3). In each river, the gauge was located several km upstream of the outlet and thus missed small tributaries near the mouth. Consequently, we scaled up from discharge estimates at the gauges to discharge estimates at the watershed outlets using the watershed to gauged area ratios (the Homathko watershed is 98 % gauged, whereas the Southgate watershed is 87 % gauged).

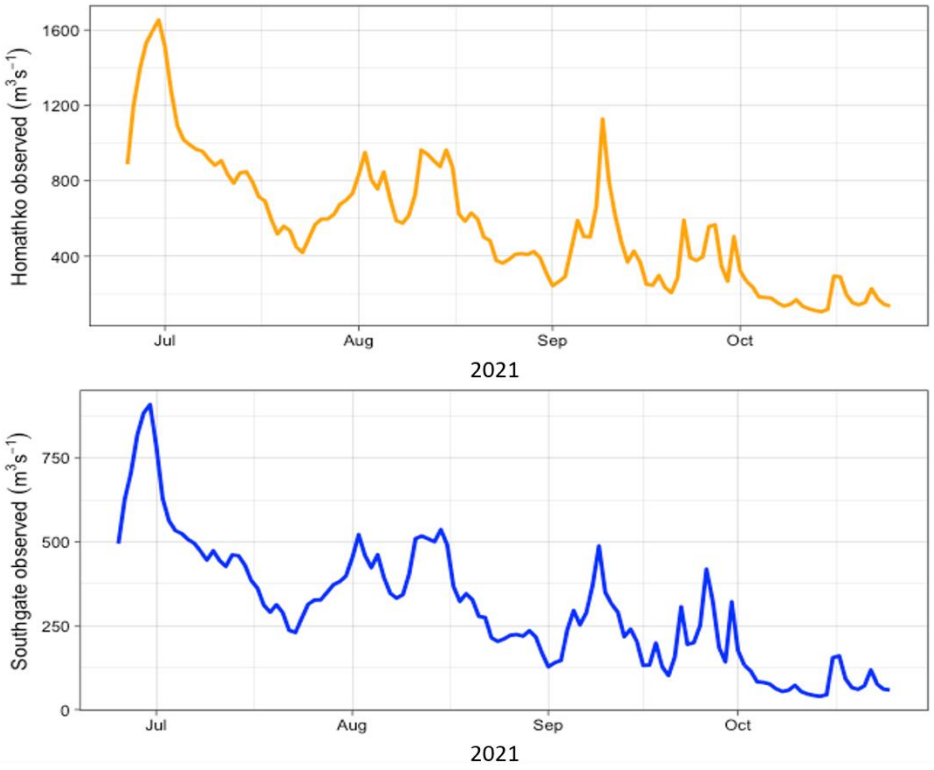

Figure S1. Flow discharge data collected between June 2021 and October 2021 by the Water Survey of Canada gauging stations on the Homathko and Southgate Rivers.

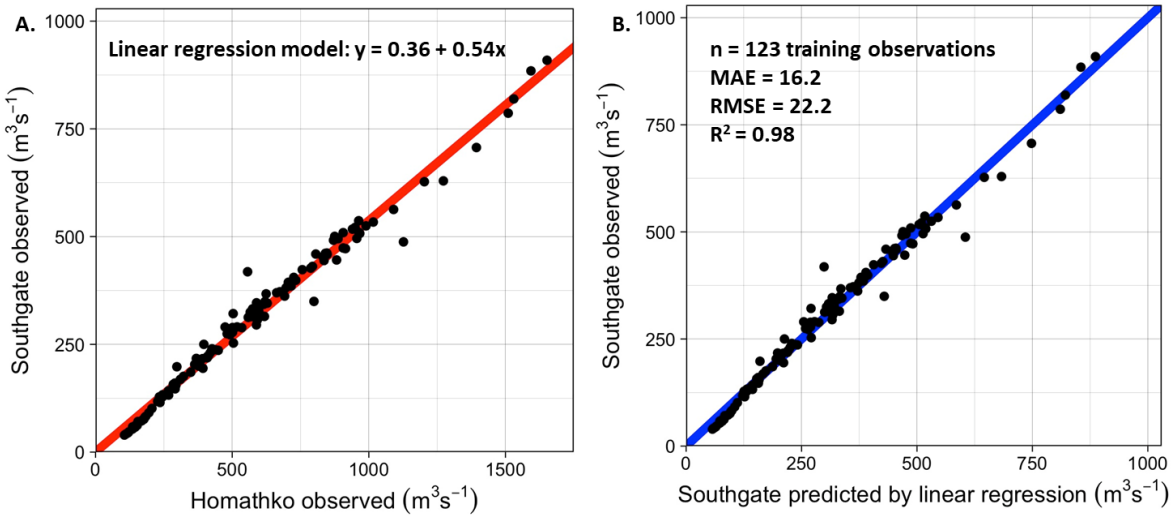

Figure S2. A. Relationship between flow discharge observations in the Homathko and Southgate River in 2021. **B.** Comparison between Southgate flow predicted by linear regression (in A) and Southgate flow observed at the gauging station (Fig. S1). The blue line is a 1:1 line representing 100% accurate prediction. MAE = mean absolute error, RMSE = root-mean-squared error, R^2 = coefficient of determination.

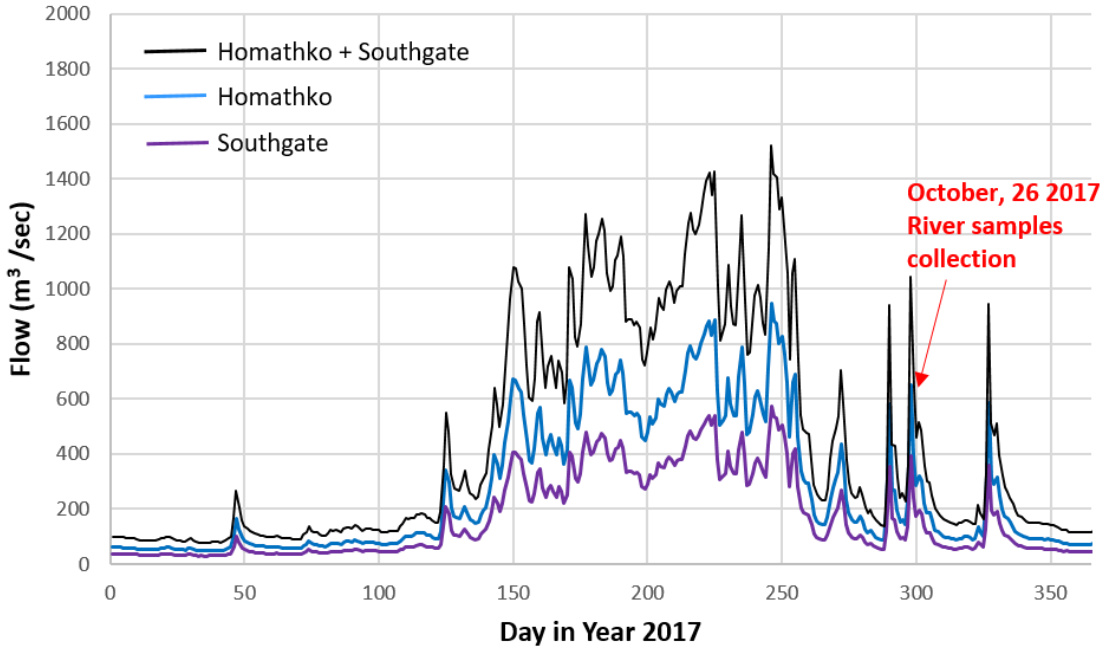

Figure S3. Flow discharge for the Homathko and Southgate Rivers observed and modelled for the year 2017.

Text S2: Bedload discharge of the Homathko and Southgate Rivers

Bedload discharge for the Homathko River was estimated at 99 kg/sec by Syvitski and Farrow (1983) which equates to 3122 x 10^6 kg/yr. No estimate was found in the literature for the Southgate river bedload discharge. We thus used the ratio between the two river watersheds (Eq. 1) as a scaling factor to deduce an annual mean river bedload for the Southgate using the Homathko bedload estimate. This gives a Southgate bedload annual discharge of 1073 x 10^6 kg/yr. In total, the bedload discharge brought in by the two rivers equals 4164 Kt/yr.

Because the Southgate bedload discharge is estimated based on the Homathko bedload discharge, we use the average total organic carbon of the samples collected in the bedload of both rivers (i.e. TOC = 0.35 ± 0.1 %, Table S7) to derive a total OC bedload flux. This gives a total organic carbon bedload flux of 14.9 ± 3.6 Kt OC /yr for the Homathko and Southgate rivers.

$$\frac{5782}{1985}\frac{km^2}{km^2} = 2.91$$

Equation S1. Ratio between the Homathko and the Southgate Rivers' watersheds

$$\frac{3122}{2.91} \text{ x } 10^6 \text{ kg/yr} = 1073 \text{ x } 10^6 \text{ kg/yr}$$

Equation S2. Southgate River annual bedload flux predicted based on the Homathko River bedload flux

Syvitski, J. P. M., & Farrow, G. E. (1983). Structures and processes in Bayhead Deltas: Knight and Bute Inlet, British Columbia. Sedimentary Geology, 36(217), 244.

Text S3: Total suspended sediment (TSS) load discharge of the Homathko and Southgate Rivers

A total of 34 and 20 suspended sediment samples were collected by the Hakai Institute between 2016 and 2021 in the Homathko and Southgate Rivers, respectively (Tables S1 and S2). Constituent concentrations and flow discharge were measured for each sample. Based on these physical samples and on the water discharge data presented in Text S1, we modeled monthly and annual constituent fluxes using the USGS LOADEST program (Runkel et al., 2004). LOADEST uses a time series of paired streamflow and constituent concentration data to construct a calibration regression, which is then applied to a daily discharge record to obtain daily constituent fluxes (load; mass day-1). The program uses a series of models which are nested within Equation S3.

$$\ln Load = a_0 + a_1 \ln Q + a_2 \ln Q^2 + a_3 \sin(2\pi dtime) + a_4 \cos(2\pi dtime) + a_5 dtime + a_6 dtime^2$$

Equation S3. Equation used by the LOADEST program to model monthly and annual TSS discharge for the Homathko and Southgate Rivers. lnLoad = the natural log of Load, lnQ = [ln(streamflow) - center of ln(streamflow)], and dtime = [decimal time - center of decimal time].

We used the AIC criteria to select the model of best fit from among the nested series of potential models, following common practice when there is no a priori reason for model preference (Burnham and Anderson, 2002).

In total, we estimate an annual mean suspended load of 30.9 kg/sec for the Homathko River, averaged between years 2016 to 2020. This number is almost equal to the previous estimate of 29 kg/sec made on the Homathko River by Syvitski and Farrow (1983). The annual mean suspended load of the Southgate River is estimated at 7 kg/sec averaged between 2017 and 2020.

Runkel, R.L., Crawford, C.G., and Cohn, T.A., 2004, Load Estimator (LOADEST): A FORTRAN Program for Estimating Constituent Loads in Streams and Rivers: U.S. Geological Survey Techniques and Methods Book 4, Chapter A5, 69 p.

Burnham, K. P., & Anderson, D. R., 2002. A practical information-theoretic approach. Model selection and multimodel inference, 2.

Syvitski, J. P. M., & Farrow, G. E. (1983). Structures and processes in Bayhead Deltas: Knight and Bute Inlet, British Columbia. Sedimentary Geology, 36(217), 244.

Site	Date	Time	Flow (ft^3/sec)	Conc. (mg/l)
Homathko	04/30/2016	1200	7275	37,4
Homathko	06/02/2018	1200	10877	46,6
Homathko	07/31/2018	1200	32454	316,0
Homathko	08/29/2018	1200	20129	70,5
Homathko	09/19/2018	1200	5544	5,2
Homathko	10/23/2018	1200	3521	7,1
Homathko	11/27/2018	1200	8581	62,5
Homathko	01/28/2019	1200	1978	4,4
Homathko	05/16/2019	1200	9712	41,4
Homathko	06/25/2019	1200	12784	36,8
Homathko	07/16/2019	1200	18717	58,3
Homathko	08/22/2019	1200	19882	219,7
Homathko	09/19/2019	1200	9217	78,8
Homathko	10/10/2019	1200	4202	32,2
Homathko	10/18/2019	1200	6427	38,8
Homathko	11/07/2019	1200	3267	13,5
Homathko	12/05/2019	1200	2423	8,0
Homathko	01/21/2020	1200	2373	31,9
Homathko	02/18/2020	1200	1801	3,0
Homathko	03/16/2020	1200	1434	2,6
Homathko	06/03/2020	1200	12643	55,7
Homathko	07/09/2020	1200	17340	66,6
Homathko	08/12/2020	1200	12572	91,6
Homathko	10/22/2020	1200	5756	33,8
Homathko	12/17/2020	1200	3955	9,0
Homathko	01/13/2021	1200	3343	14,9
Homathko	02/09/2021	1200	1711	4,0
Homathko	03/10/2021	1200	1518	3,3
Homathko	04/20/2021	1200	5240	21,2
Homathko	05/20/2021	1200	7500	29,0
Homathko	06/15/2021	1200	14630	73,1
Homathko	07/13/2021	1200	29709	162,1
Homathko	08/11/2021	1200	34016	238,6
Homathko	10/07/2021	1200	5372	17,6

Table S1. Suspended sediment samples collected in the Homathko River between 2016 and 2021. Flow discharge are given in cubic feet per second and concentrations (Conc.) in milligram per liter)

Site	Date	Time	Flow (ft^3/sec)	Conc. (mg/l)
Southgate	04/30/2018	1200	3915	16,5
Southgate	06/02/2018	1200	5847	29,9
Southgate	08/29/2018	1200	10810	37,9
Southgate	09/19/2018	1200	2987	3,5
Southgate	10/23/2018	1200	1901	6,1
Southgate	03/28/2019	1200	1280	2,9
Southgate	06/25/2019	1200	6870	25,1
Southgate	12/17/2020	1200	2134	5,7
Southgate	01/13/2021	1200	1806	4,4
Southgate	02/09/2021	1200	931	3,1
Southgate	03/10/2021	1200	827	2,3
Southgate	04/20/2021	1200	2824	13,3
Southgate	05/20/2021	1200	4035	47,7
Southgate	06/15/2021	1200	7860	88,2
Southgate	06/30/2021	1200	32107	526,4
Southgate	07/13/2021	1200	16288	61,3
Southgate	08/10/2021	1200	14314	131,7
Southgate	08/11/2021	1200	18010	237,9
Southgate	09/30/2021	1200	11347	49,9
Southgate	10/07/2021	1200	2192	35,7

Table S2. Suspended sediment samples collected in the Southgate River between 2018 and 2021. Flow discharge are given in cubic feet per second and concentrations (Conc.) in milligram per liter)

Text S4: Sedimentation rate based on bathymetric difference maps

The first approach to determine sedimentation rates in Bute Inlet uses differences between two bathymetric surveys obtained in 2008 and 2018, and analyzed by Heijnen et al. (in review). This approach derived sediment volumes in the channel and lobe of Bute Inlet, showing that sediment is transported stepwise down the channel as a result of turbidity currents becoming less frequent along the channel transect. Previous work in the same channel highlighted zones of erosion and deposition that migrate upstream significantly (100 to 450 m per year) due to the presence of turbidity current-related knickpoints (Heijnen et al., 2020). Overall, the channel has a net eroded volume of 41 ± 12 Mm^3 and a net deposited volume of 19 ± 12 Mm^3 between 2008 and 2018 (Table S3; Heijnen et al., in review). The lobe shows no erosion and a total deposition of 30 ± 38 Mm^3 between 2008 and 2018 (Table S3; Heijnen et al., in review). Volume uncertainties are based on vertical accuracy of the multibeam surveys of 0.5 % of the water depth, hence the 600 m deep lobe is greatly affected (Heijnen et al., 2020). We divided these net 2008-2018 sediment volumes by the surface areas of the channel and lobe, to derive annual sedimentation rates of -16 ± 9 cm/yr and 18 ± 9 cm/yr, respectively (Table S4).

Comparison between the sources of sediment available in the Bute submarine system (i.e. supplied by the rivers and made available through erosion in the channel; Table S4) and sediment deposited on the seabed on the channel and lobe results in a sediment deficit of 3.1 ± 0.9 Mm^3/yr (Table S4). If we assume that this deficit is spread over the overbanks and distal flat basin (i.e. outside of channe and lobe; Heijnen et al., in review), and that we divide this deficit by the surface area of the overbanks and distal flat basin, we find a sedimentation rate of 2 ± 0.6 cm/yr in these two sub-environments (Table S4).

Heijnen, M. S., Clare, M.A., Cartigny, M. J., Talling, P.J., Hage, S., Pope, E.L., Bailey, L., Sumner, E.J., Lintern, D.G., Stacey, C.D., Parsons, D.P., Simmons, S.M., Chen, Y., Hubbard, S.M., Eggenhuisen, J.T., Kane, I., Hughes Clarke, J.E. (in review, EPSL) Fill, flush or shuffle: How is sediment carried through submarine channels to build lobes?

Heijnen, M. S., Clare, M. A., Cartigny, M. J., Talling, P. J., Hage, S., Lintern, D. G., Stacey, C.D., Parsons, D.R., Simmons, S.M., Chen, Y., Sumner, E.J., Dix, J.K., Hughes Clarke, J.E. (2020). Rapidly-migrating and internally-generated knickpoints can control submarine channel evolution. Nature communications, 11(1), 1-15.

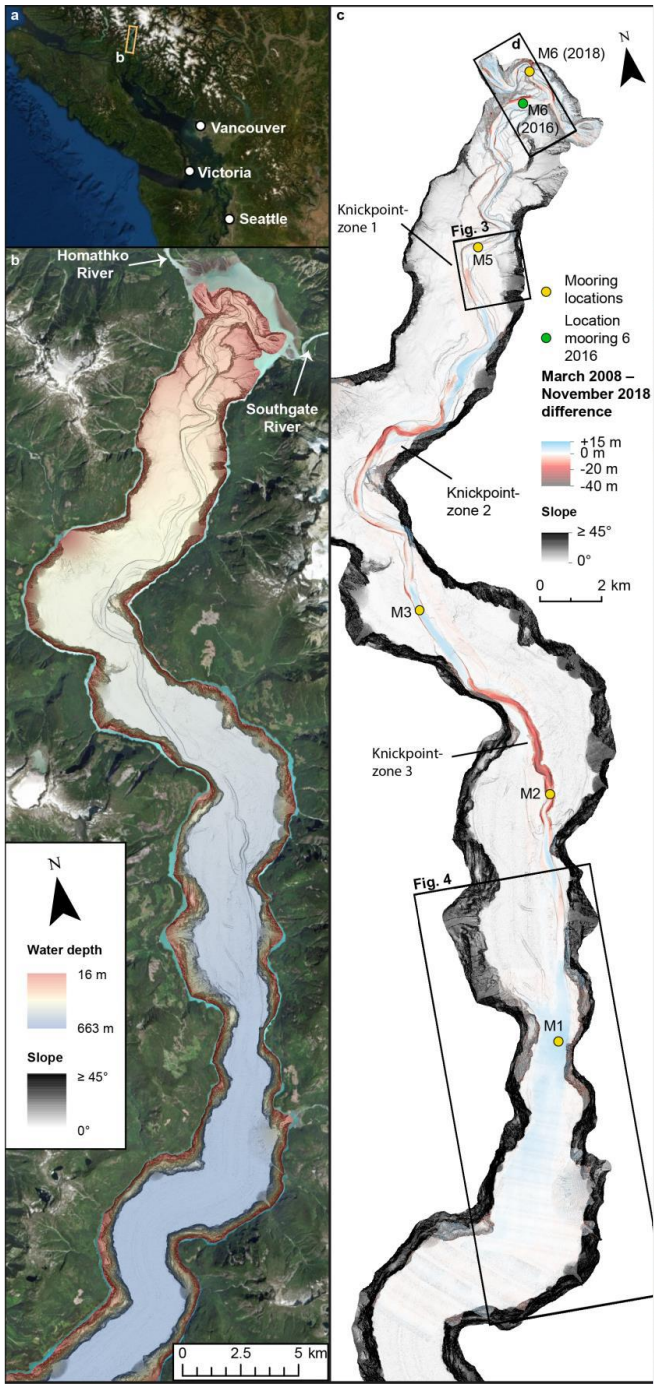

Figure S4. Location, bathymetry and 2008 to 2018 difference maps modified from Heijnen et al. (in review). **A.** Location of Bute Inlet. **B.** Overview of the submarine channel-lobe system in Bute Inlet as monitored in March 2008. Data is presented as a slope map overlain by a semi-transparent bathymetry map. **C.** 2008 slope map overlain by a March 2008 – November 2018

difference map. Note the along channel alternation of erosional and depositional areas controlled by knickpoints.

Heijnen et al. (in review)		
Sub-environment	**Volume of sediment sources 2008-2018** (eroded from seabed)	**Volume of sediment deposited on the seabed between 2008 and 2018**
Channel	41 ± 12 Mm^3	19 ± 11 Mm^3
Lobe	No net erosion	30 ± 38 Mm^3
Total	41 ± 12 Mm^3	49 Mm^3

Table S3. Sediment budgets in the channel and lobe between March 2008 and November 2018 (modified from Heijnen et al., in review).

Sub-environment	Annual net sediment volume budget (Mm^3/yr)	Surface area (km^2)	Annual sedimentation rate (cm/yr)
Homathko and Southgate Rivers	3.8 ± 2.5	n/a	n/a
Channel	-2.0 ± 1 (-3.7 + 1.7)	12.2	**-16 ± 9**
Lobe	2.7 ± 3.4	15.4	**18 ± 22**
Total sediment sources (i.e. eroded from seabed and supplied by rivers)	7.5 ± 3.6	n/a	n/a
Total deposited sediment	4.5 ± 4.5	n/a	n/a
Deficit between sources and deposits	3.1 ± 0.9	n/a	n/a
Deficit spread over overbanks and distal flat basin	3.1 ± 0.9	133	**2.3 ± 0.6**

Table S4. Annual sediment budgets and annual sedimentation rates in the Bue Inlet sub-environments, obtained based on time-lapse bathymetry presented in Heijnen et al. (in review; Table S3). Sediment volume delivered by the rivers is represented as the river sediment load volume if it were deposited using a sediment density of 2585 kg/m^3 and a porosity of 30 to 60 %.

Text S5: Sedimentation rates based on ^{210}Pb dating

A second approach, holding for a centennial timescale, was used to determine sedimentation rates in the Bute Inlet sub-environments, based on previous work (Syvistki et al., 1988; Heerema, 2021). ^{210}Pb dating was performed in Bute Inlet on five sediment cores collected in the overbanks and on one sediment core collected in the distal flat basin (Fig. S5). A sedimentation model was also developed on two sediment cores in the overbanks by Syvitski et al. (1987), allowing comparison between two methods on these cores (Fig. S5, Table S4). We computed the average between the sedimentation rates presented in Syvistki et al. (1988) and Heerema (2021), to derive a mean sedimentation rate of 2 ± 1.5 cm/yr in the overbanks and 1 ± 0.3 cm/yr in the distal flat basin (Table S4). These sedimentation rates are lower compared to the sedimentation rates derived for the overbanks and distal flat basin by time-lapse bathymetry (i.e. Approach 1; Text S4). This trend of falling mean sedimentation rate with increasing time span was previously highlighted globally, under the so-called "Sadler effect" (Sadler, 1981).

Mean sedimentation rate in the depositional lobe is also expected to decrease with increasing time span for which the lobe is considered (Sadler, 1981). No dating was performed on the cores collected in the lobe, nor the channel, as these environments are too sandy. Instead, we used an assumed relationship between the sedimentation rate obtained in the overbank and that of the channel and lobe (Equations S4 and S5).

$$\mathbf{C_{SR}} = 0.35 * O_{SR} = 0.35 * 2 \pm 1.5 = \mathbf{0.7} \pm 0.5 \ \mathbf{cm/yr}$$

Equation S4. Assumed relationship between sedimentation rate in the channel (C_{SR}) and in the overbank (O_{SR})

$$\mathbf{L_{SR}} = 5 * O_{SR} = 5 * 2 \pm 1.5 = \mathbf{10} \pm 7.5 \ \mathbf{cm/yr}$$

Equation S5. Assumed relationship between sedimentation rate in the lobe (L_{SR}) and in the overbank (O_{SR})

These relationships are based on the relationships between overbanks and channel/lobe found in the Congo turbidity current system (Baudin et al., 2020). We acknowledge that the Congo system is different (e.g. scale, composition) compared to the Bute system. However, Baudin et al. (2020) is the only study, to our knowledge, that provides separate sedimentation rates for the different turbidity current sub-environments over centennial timescales. Furthermore, it seems reasonable to assume that the Bute channel will likely reach a net positive sedimentation rate

close to zero over centennial timescales. Indeed, if the channel were to keep a negative sedimentation rate (as suggested by the time-lapse bathymetry in Text S4), we would expect to see a canyon rather than a channel in the Bute turbidity current system (Deptuck et al., 2003). The 10 cm/yr sedimentation rate found in the lobe for a centennial timescale is lower compared to the 18 cm/yr found for a decennial timescale (Text S4), which is line with the Sadler effect (Sadler, 1981).

Baudin, F., Rabouille, C., & Dennielou, B. (2020). Routing of terrestrial organic matter from the Congo River to the ultimate sink in the abyss: a mass balance approach (André Dumont medallist lecture 2017). Geologica Belgica, 23(1-2).

Deptuck, M.E., Steffens, G.S., Barton, M., Pirmez, C. (2003) Architecture and evolution of upper fan channel-belts on the Niger Delta slope and in the Arabian Sea. Marine and Petroleum Geology 20, 649-676.

Heerema, C. J. (2021). Evolution of Turbidity Currents: New insights from direct field measurements, Durham theses, Durham University. Available at Durham E-Theses Online: http://etheses.dur.ac.uk/13963/

Sadler, P. M. (1981). Sediment Accumulation Rates and the Completeness of Stratigraphic Sections. The Journal of Geology, 89(5), 569–584. doi:10.1086/628623

Syvitski, J. P. M., Smith, J.N., Calabrese, E.A., Boudreau, B.P. (1988). Basin Sedimentation and the Growth of Prograding Deltas. Journal of Geophysical Research, 93 (C6), 6895-6908.

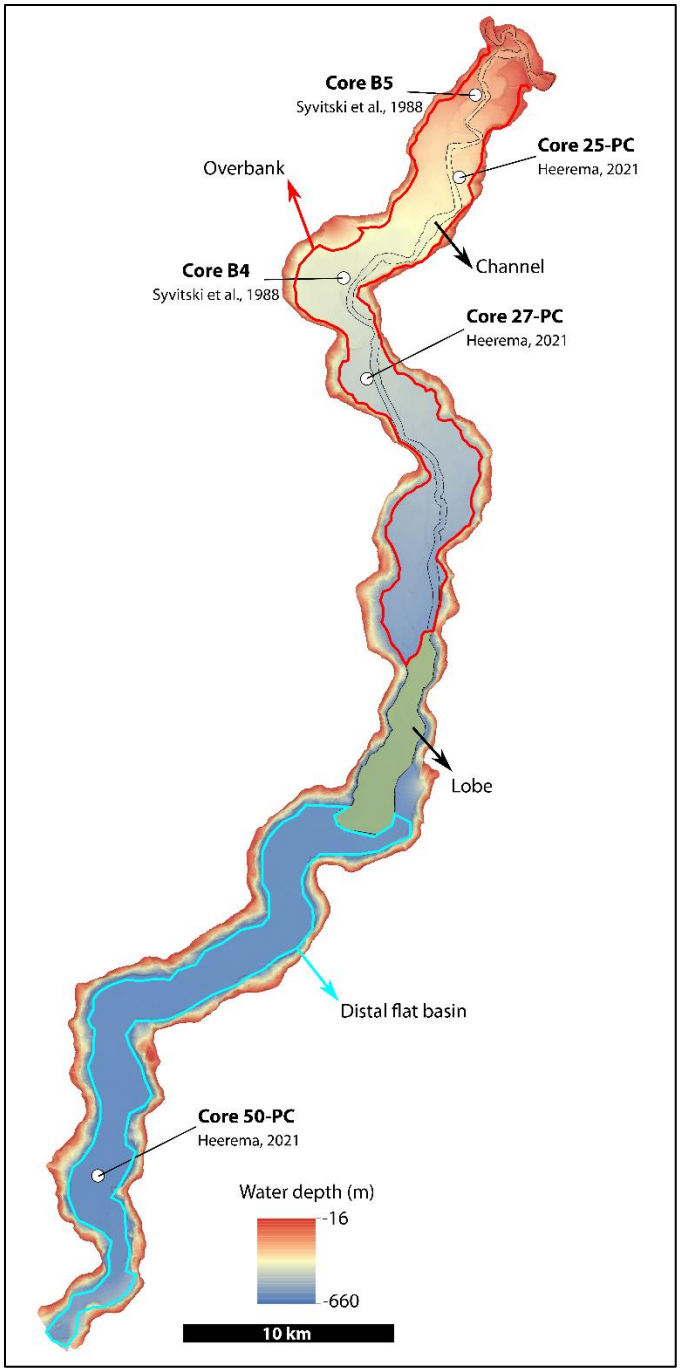

Figure S5. Location of the sediment cores previously dated by Syvitski et al. (1988) and Heerema (2021).

Core and reference	^{210}Pb sedimentation rate (cm/yr)	Model sedimentation rate (cm/yr)	Sub-environment (Location Fig. S5)	Average (cm/yr)
B5 Syvistki et al., 1988	4.56	3.78	Overbanks	**2 ± 1.5** (n=7)
25-PC Heerema, 2021	1.2 (γ) 0.9 (α)	-	Overbanks	
B4 Syvistki et al., 1988	1.14	1.11	Overbanks	
27-PC Heerema, 2021	0.9 (γ)	-	Overbanks	
50-PC Heerema, 2021	0.9 (γ) 1 (α)	-	Distal flat basin	**1 ± 0.5** (n=2)

Table S5. ^{210}Pb-determined and modelled sedimentation rates on five sediment cores displayed in Fig. S5 (Syvistki et al., 1988, Heerema, 2021). Gamma (γ) and alpha (α) spectrometry sedimentation are given where calculated

Text S6: Mixing model to determine the terrestrial versus marine organic carbon contribution in the samples collected from the fjord distal flat basin

We have used a simple binary (i.e. 2 end-members) mixing model to discriminate between terrestrial and marine organic carbon in the samples collected from the fjord distal flat basin. The carbon stable isotopes compositions ($\delta^{13}C$) of each sample and of two fixed end-members were used to run the model, following equations S6 and S7 (Hilton et al., 2015).

$$F_{terr} = \frac{\delta^{13}C_{sample} - \delta^{13}C_{mar}}{\delta^{13}C_{terr} - \delta^{13}C_{mar}} \times 100$$

Equation S6. Equation used to derive the fraction of terrestrial organic carbon contained in a sample.

$$F_{terr} + F_{mar} = 100$$

Equation S7. The contribution of marine and terrestrial organic carbon represents 100 % of the total organic carbon held in a sample.

Where:

- F_{terr} is the fraction of terrestrial organic carbon in %,
- F_{mar} is the fraction of marine organic carbon in %,
- $\delta^{13}C_{sample}$ is the measured carbon stable isotope composition of a sample in ‰,
- $\delta^{13}C_{mar}$ is the carbon stable isotope composition of the marine end-member, fixed at -20.5 ‰ (i.e., the minimum value measured on samples collected in the distal basin core)
- $\delta^{13}C_{terr}$ is the carbon stable isotope composition of the terrestrial end-member, fixed at -27 ‰ (Hecky and Hesslein, 1995)

Applying these equations to the samples collected in the distal flat basin results in a mean relative terrestrial contribution of 46 % (Table S6). Therefore, we estimate that about 44 % of the organic carbon found in the upper two meter sediment of the distal flat basin is of marine origin.

Hecky, R.E. and Hesslein, R.H. Contributions of Benthic Algae to Lake Food Webs as Revealed by Stable Isotope Analysis (1995). *J. N. Am. Benthol. Soc.,* 14(4):631-653

Hilton, R., Galy, V., Gaillardet, J. et al. Erosion of organic carbon in the Arctic as a geological carbon dioxide sink. Nature 524, 84–87 (2015). https://doi.org/10.1038/nature14653

Macdonald, R., Macdonald, D., O'Brien, M., & Gobeil, C. (1991). Accumulation of heavy metals (Pb, Zn, Cu, Cd), carbon and nitrogen in sediments from Strait of Georgia, BC, Canada. Marine Chemistry, 34(1-2), 109-135.

Sample depth (cm)	$\delta^{13}C_{sample}$ (‰)	F_{terr} (%)	F_{mar} (%)
20	-23,01	39	61
21	-23,37	44	56
30	-25,69	80	20
33	-25,83	82	18
37	-22,18	26	74
57	-25,25	73	27
63	-24,11	56	44
73	-21,79	20	80
86	-23,99	54	46
90	-26,03	85	15
104	-23,93	53	47
121	-23,72	50	50
151	-23,29	43	57
177	-22,40	29	71
183	-20,51	0	100
196	-22,55	32	68
197	-22,53	31	69
200	-22,17	26	74
	Mean	**46**	**54**

Table S6. Mixing model applied on sediment samples collected in the distal flat basin of Bute Inlet (i.e. core 15 in Fig. 3) following Equations S6 and S7. $\delta^{13}C$ = carbon stable isotope composition measured on each sample. F_{terr} = fraction of terrestrial organic carbon in each sample. F_{mar} = fraction of marine organic carbon in each sample.

Cruise number	Sample code	River	Environment	TOC (%)	$\delta^{13}C$ (‰)[a]	R (^{14}C yr)[b]	D_{50} (µm)	D_{90} (µm)	Latitude (°)	Longitude (°)
PGC-2017-005	RW18a	Homathko	water column	0.70	-25.05	29	45	155	50.948	-124.861
PGC-2017-005	RW20	Homathko	water column	0.64	-23.85		37	247	50.934	-124.863
PGC-2017-005	RB16	Homathko	river bank	0.09	-27.04		104	207	50.941	-124.857
PGC-2017-005	RB18	Homathko	river bank	0.17	-26.78		78	185	50.948	-124.861
PGC-2017-005	RB22	Homathko	river bank	0.25	-27.19		65	174	50.941	-124.857
PGC-2017-005	RD6	Homathko	delta	0.18	-26.71		75	230	50.9	-124.9
PGC-2017-005	RD8	Homathko	delta	0.04	-27.21		347	770	50.919	-124.848
PGC-2017-005	RP7a	Homathko	plume	1.77	-17.15		26	140	50.919	-124.848
PGC-2017-005	RP9a	Homathko	plume	2.90	-16.27				50.919	-124.848
PGC-2017-005	RP11a	Homathko	plume	2.86	-13.07				50.920	-124.844
PGC-2017-005	RW16a	Homathko	plume	1.56	-16.82				50.941	-124.857
PGC-2017-005	RW17a	Homathko	plume	1.82	-18.60				50.944	-124.858
PGC-2017-005	RW23a	Southgate	water column	1.42	-25.24				50.886	-124.797
PGC-2017-005	RW23b	Southgate	water column	0.85	-25.83	795	13	56	50.886	-124.797
PGC-2017-005	RW23c	Southgate	water column	0.91	-25.56				50.886	-124.797
PGC-2017-005	RW23d	Southgate	water column	0.70	-25.91		39	209	50.886	-124.797
PGC-2017-005	RB24	Southgate	river bank	0.69	-27.45		173	331	50.888	-124.797
PGC-2017-005	RD12	Southgate	delta	0.41	-26.23		37	159	50.891	-124.804
PGC-2017-005	RD14	Southgate	delta	0.57	-26.74		183	493	50.895	-124.800
PGC-2017-005	RP13a	Southgate	plume	3.14	-19.44				50.891	-124.804
PGC-2017-005	RP15a	Southgate	plume	4.99	-17.95				50.895	-124.800
PGC-2017-005	RW19a	Southgate	plume	1.27	-19.82		33	214	50.938	-124.855

Table S7. Organic geochemistry, grain size, location and metadata associated with the river samples presented in this study. a: carbon stable isotopes $\delta^{13}C$ values are reported relative to Vienna Pee-Dee Belemnite (VDBP). b: R stands for reservoir age offset, reported in ^{14}C years and calculated following Soulet et al. (2016).

Core number in paper	Cruise number	Station number	Core type	Depth in core (cm)	Sub-Environment	TOC (%)	$\delta^{13}C$ (‰)[a]	R (^{14}C yr)[b]	D_{50} (µm)	D_{90} (µm)	Latitude (°)	Longitude (°)	Water depth (m)
1	PGC-2016-007	STN028	Box	3 to 7	Channel	0.03	-27.3				50.904	-124.834	227
1	PGC-2016-007	STN028	Box	20 to 24	Channel	0.19	-27.7				50.904	-124.834	227
1	PGC-2016-007	STN028	Box	4	Channel	0.26	-26.9		84	169	50.904	-124.834	227
1	PGC-2016-007	STN028	Box	9	Channel	0.03	-25.7		262	1214	50.904	-124.834	227
1	PGC-2016-007	STN028	Box	12	Channel	0.08	-26.3		624	1348	50.904	-124.834	227
1	PGC-2016-007	STN028	Box	18	Channel	0.04	-25.5		466	1333	50.904	-124.834	227
1	PGC-2016-007	STN028	Box	32	Channel	0.02	-26.3		413	1329	50.904	-124.834	227
2	PGC-2016-007	STN015	Box	2 to 6	Channel	0.27	-27.2				50.864	-124.864	319
2	PGC-2016-007	STN015	Box	18 to 22	Channel	0.03	-24.7				50.864	-124.864	319
3	PGC-2016-007	STN010	Box	0 to 4	Channel	0.37	-27.6				50.865	-124.868	322
3	PGC-2016-007	STN010	Box	15 to 19	Channel	2.70	-27.0				50.865	-124.868	322
3	PGC-2016-007	STN010	Box	24 to 28	Channel	0.03	-25.5				50.865	-124.868	322
3	PGC-2016-007	STN010	Box	2	Channel	0.35	-27.8		41	124	50.865	-124.868	322
3	PGC-2016-007	STN010	Box	6	Channel	0.55	-27.5		77	189	50.865	-124.868	322
3	PGC-2016-007	STN010	Box	20	Channel	0.03	-26.1				50.865	-124.868	322
3	PGC-2016-007	STN010	Box	26	Channel	0.02	-26.1				50.865	-124.868	322
4	PGC-2016-007	STN014	Box	0 to 4	Channel	0.03	-26.1				50.862	-124.870	322
4	PGC-2016-007	STN014	Box	17 to 21	Channel	0.03	-26.3				50.862	-124.870	322
5	PGC-2016-007	STN019	Box	1	Channel	0.56	-27.5	997	12	52	50.763	-124.915	477
5	PGC-2016-007	STN019	Box	4	Channel	0.68	-27.7	71	59	171	50.763	-124.915	477
5	PGC-2016-007	STN019	Box	10	Channel	0.92	-27.8	71			50.763	-124.915	477
5	PGC-2016-007	STN019	Box	13	Channel	0.02	-26.7		81	157	50.763	-124.915	477
5	PGC-2016-007	STN019	Box	20	Channel	0.06	-26.0	2680	172	332	50.763	-124.915	477
5	PGC-2016-007	STN019	Box	28	Channel	0.02	-25.4	3600	265	1248	50.763	-124.915	477
6	PGC-2016-007	STN014	Box	0 to 4	Channel	0.03	-26.1				50.862	-124.870	322
6	PGC-2016-007	STN014	Box	17 to 21	Channel	0.03	-26.3				50.862	-124.870	322
6	PGC-2016-007	STN025	Box	1	Channel	1.53	-28.4				50.704	-124.868	570
6	PGC-2016-007	STN025	Box	5	Channel	0.03	-26.5		70	145	50.704	-124.868	570
6	PGC-2016-007	STN025	Box	10	Channel	0.03	-26.3		78	142	50.704	-124.868	570
6	PGC-2016-007	STN025	Box	15	Channel	0.02	-26.2		109	209	50.704	-124.868	570
6	PGC-2016-007	STN025	Box	18	Channel	0.02	-26.0		193	350	50.704	-124.868	570
6	PGC-2016-007	STN025	Box	22	Channel	0.02	-26.7		316	1289	50.704	-124.868	570
7	PGC-2016-007	STN036	Box	1	Lobe	0.76	-26.8		23	104	50.633	-124.881	611
7	PGC-2016-007	STN036	Box	3	Lobe	0.42	-26.7		17	83	50.633	-124.881	611
7	PGC-2016-007	STN036	Box	4	Lobe	1.53	-27.9		61	179	50.633	-124.881	611
7	PGC-2016-007	STN036	Box	5	Lobe	0.33	-27.4				50.633	-124.881	611
7	PGC-2016-007	STN036	Box	6	Lobe	0.05	-25.5		82	160	50.633	-124.881	611
7	PGC-2016-007	STN036	Box	10	Lobe	0.03	-25.2		145	298	50.633	-124.881	611
7	PGC-2016-007	STN036	Box	15	Lobe	0.08	-27.7		137	296	50.633	-124.881	611
7	PGC-2016-007	STN036	Box	20	Lobe	0.08	-27.0		116	279	50.633	-124.881	611
7	PGC-2016-007	STN036	Box	24	Lobe	0.03	-26.5		164	1151	50.633	-124.881	611
8	PGC-2016-007	STN032	Box	10 to 14	Overbank	0.15	-26.8				50.903	-124.834	218
8	PGC-2016-007	STN032	Box	20 to 24	Overbank	0.30	-27.0				50.903	-124.834	218
8	PGC-2016-007	STN032	Box	15	Overbank	0.18	-27.5				50.903	-124.834	218
8	PGC-2016-007	STN032	Box	20	Overbank	0.17	-26.7				50.903	-124.834	218
8	PGC-2016-007	STN032	Box	22	Overbank	0.31	-26.8				50.903	-124.834	218
9	PGC-2016-007	STN031	Box	6 to 10	Overbank	0.27	-26.7				50.902	-124.835	189
9	PGC-2016-007	STN031	Box	16 to 20	Overbank	0.26	-26.7				50.902	-124.835	189
9	PGC-2016-007	STN031	Box	12	Overbank	0.26	-26.3		11	45	50.902	-124.835	189
9	PGC-2016-007	STN031	Box	24	Overbank	0.34	-27.4		13	59	50.902	-124.835	189

Table S8. Organic geochemistry, grain size, location and metadata associated with the samples collected in Bute Inlet presented in this study. a: carbon stable isotopes $\delta^{13}C$ values are reported relative to Vienna Pee-Dee Belemnite (VDBP). b: R stands for reservoir age offset, reported in ^{14}C years and calculated following Soulet et al. (2016).

Core number in paper	Cruise number	Station number	Core type	Depth in core (cm)	Sub-Environment	TOC (%)	$\delta^{13}C$ (‰)[a]	R (^{14}C yr)[b]	D_{50} (µm)	D_{90} (µm)	Latitude (°)	Longitude (°)	Water depth (m)
10	PGC-2016-007	STN029	Box	25	Overbank	0.38	-27.1				50.905	-124.833	223
10	PGC-2016-007	STN030	Box	5 to 9	Overbank	0.16	-27.3				50.903	-124.839	218
10	PGC-2016-007	STN030	Box	14 to 18	Overbank	0.27	-27.3				50.903	-124.839	218
10	PGC-2016-007	STN030	Box	7	Overbank	0.46	-27.2				50.903	-124.839	218
10	PGC-2016-007	STN030	Box	11	Overbank	0.11	-26.7				50.903	-124.839	218
10	PGC-2016-007	STN030	Box	25	Overbank	0.23	-27.0				50.903	-124.839	218
10	PGC-2016-007	STN030	Box	30	Overbank	0.21	-27.0				50.903	-124.839	218
11	PGC-2016-007	STN09	Box	0 to 4	Overbank	0.20	-27.6				50.864	-124.867	321
11	PGC-2016-007	STN09	Box	20 to 24	Overbank	0.02	-26.0				50.864	-124.867	321
11	PGC-2016-007	STN09	Box	5	Overbank	0.40	-27.9				50.864	-124.867	321
11	PGC-2016-007	STN09	Box	13	Overbank	0.10	-29.1				50.864	-124.867	321
11	PGC-2016-007	STN09	Box	15	Overbank	0.35	-27.7				50.864	-124.867	321
11	PGC-2016-007	STN09	Box	20	Overbank	0.27	-27.2				50.864	-124.867	321
11	PGC-2016-007	STN09	Box	24	Overbank	0.02	-26.0				50.864	-124.867	321
11	PGC-2016-007	STN09	Box	30	Overbank	0.38	-28.2				50.864	-124.867	321
12	PGC-2016-007	STN020	Box	2	Overbank	0.31	-26.2		69	155	50.763	-124.911	466
12	PGC-2016-007	STN020	Box	7	Overbank	0.04	-26.2				50.763	-124.911	466
12	PGC-2016-007	STN020	Box	12	Overbank	0.17	-26.0		46	134	50.763	-124.911	466
12	PGC-2016-007	STN020	Box	23	Overbank	0.03	-25.8		116	225	50.763	-124.911	466
12	PGC-2016-007	STN020	Box	32	Overbank	0.42	-26.8		22	89	50.763	-124.911	466
13	PGC-2016-007	STN021	Box	10 to 14	Overbank	0.02	-25.7				50.762	-124.918	462
13	PGC-2016-007	STN021	Box	20 to 24	Overbank	0.24	-26.6				50.762	-124.918	462
13	PGC-2016-007	STN021	Box	16	Overbank	0.25	-26.9				50.762	-124.918	462
13	PGC-2016-007	STN021	Box	9	Overbank	0.03	-24.8				50.762	-124.918	462
14	PGC-2016-007	STN026	Box	10 to 14	Overbank	0.17	-26.1				50.705	-124.865	538
14	PGC-2016-007	STN026	Box	24 to 28	Overbank	0.30	-25.9				50.705	-124.865	538
14	PGC-2016-007	STN026	Box	8	Overbank	0.33	-26.9		35	105	50.705	-124.865	538
14	PGC-2016-007	STN026	Box	14	Overbank	0.84	-28.2		125	256	50.705	-124.865	538
14	PGC-2016-007	STN026	Box	20	Overbank	0.40	-26.3				50.705	-124.865	538
14	PGC-2016-007	STN026	Box	26	Overbank	0.20	-26.7				50.705	-124.865	538
14	PGC-2016-007	STN026	Box	30	Overbank	0.10	-26.1				50.705	-124.865	538
15	PGC-2016-003	STN01	Piston	20	Distal basin	3.07	-23.01				50.420	-125.085	647
15	PGC-2016-003	STN01	Piston	21	Distal basin	2.93	-23.37				50.420	-125.085	647
15	PGC-2016-003	STN01	Piston	30	Distal basin	0.52	-25.69				50.420	-125.085	647
15	PGC-2016-003	STN01	Piston	33	Distal basin	0.52	-25.83				50.420	-125.085	647
15	PGC-2016-003	STN01	Piston	37	Distal basin	3.52	-22.18				50.420	-125.085	647
15	PGC-2016-003	STN01	Piston	57	Distal basin	0.50	-25.25				50.420	-125.085	647
15	PGC-2016-003	STN01	Piston	63	Distal basin	2.40	-24.11	523			50.420	-125.085	647
15	PGC-2016-003	STN01	Piston	73	Distal basin	2.21	-21.79				50.420	-125.085	647
15	PGC-2016-003	STN01	Piston	86	Distal basin	0.68	-23.99				50.420	-125.085	647
15	PGC-2016-003	STN01	Piston	90	Distal basin	0.46	-26.03				50.420	-125.085	647
15	PGC-2016-003	STN01	Piston	104	Distal basin	0.43	-23.93				50.420	-125.085	647
15	PGC-2016-003	STN01	Piston	121	Distal basin	0.50	-23.72				50.420	-125.085	647
15	PGC-2016-003	STN01	Piston	151	Distal basin	0.65	-23.29				50.420	-125.085	647
15	PGC-2016-003	STN01	Piston	177	Distal basin	0.57	-22.40	1080			50.420	-125.085	647
15	PGC-2016-003	STN01	Piston	183	Distal basin	2.18	-20.51	1103			50.420	-125.085	647
15	PGC-2016-003	STN01	Piston	196	Distal basin	0.61	-22.55				50.420	-125.085	647
15	PGC-2016-003	STN01	Piston	197	Distal basin	0.72	-22.53				50.420	-125.085	647
15	PGC-2016-003	STN01	Piston	200	Distal basin	0.90	-22.17				50.420	-125.085	647

Table S8 (continued). Organic geochemistry, grain size, location and metadata associated with the samples collected in Bute Inlet presented in this study. **a:** carbon stable isotopes $\delta^{13}C$ values are reported relative to Vienna Pee-Dee Belemnite (VDBP). b: R stands for reservoir age offset, reported in ^{14}C years and calculated following Soulet et al. (2016).